The Planetary Science Journal, 3:184 (12pp), 2022 August https://doi.org/10.3847/PSJ/ac7de7

Heliocentric Effects of the DART Mission on the (65803) Didymos Binary Asteroid System

Rahil Makadia[1], Sabina D. Raducan[2], Eugene G. Fahnestock[3], and Siegfried Eggl[1,4,5,6]
[1] Department of Aerospace Engineering, University of Illinois at Urbana-Champaign, Urbana, IL 61801, USA; makadia2@illinois.edu
[2] Space Research and Planetary Sciences, Physics Institute, University of Bern, Bern, 3012, Switzerland
[3] Jet Propulsion Laboratory, California Institute of Technology, Pasadena, CA 91109, USA
[4] Department of Astronomy, University of Illinois at Urbana-Champaign, Urbana, IL 61801, USA
[5] National Center for Supercomputing Applications, University of Illinois at Urbana-Champaign, Urbana, IL 61801, USA
[6] IMCCE, Paris Observatory, 77 Avenue Denfert-Rochereau, F-75014 Paris, France
Received 2022 March 1; revised 2022 June 30; accepted 2022 July 1; published 2022 August 4

Abstract

The Double Asteroid Redirect Test (DART) is NASA's first kinetic impact–based asteroid deflection mission. The DART spacecraft will act as a projectile during a hypervelocity impact on Dimorphos, the secondary asteroid in the (65803) Didymos binary system, and alter its mutual orbital period. The initial momentum transfer between the DART spacecraft and Dimorphos is enhanced by the ejecta flung off the surface of Dimorphos. This exchange is characterized within the system by the momentum enhancement parameter, β, and on a heliocentric level by its counterpart, $\beta_{\odot}$. The relationship between β and the physical characteristics of Dimorphos is discussed here. A nominal set of Dimorphos physical parameters from the design reference asteroid and impact circumstances from the design reference mission are used to initialize the ejecta particles for dynamical propagation. The results of this propagation are translated into a gradual momentum transfer onto the Didymos system barycenter. A high-quality solar system propagator is then used to produce precise estimates of the post-DART encounters between Didymos and Earth by generating updated close approach maps. Results show that even for an unexpectedly high $\beta_{\odot}$, a collision between the Didymos system and Earth is practically excluded in the foreseeable future. A small but significant difference is found in modeling the overall momentum transfer when individual ejecta particles escape the Didymos system, as opposed to imparting the ejecta momentum as a single impulse at impact. This difference has implications for future asteroid deflection campaigns, especially when it is necessary to steer asteroids away from gravitational keyholes.

Unified Astronomy Thesaurus concepts: Close encounters (255); Near-Earth objects (1092); Asteroid dynamics (2210)

1. Introduction

Current near-Earth asteroid population models suggest that even after coordinated worldwide efforts, a majority of <1 km-sized asteroids remain undiscovered (Granvik et al. 2018). Objects larger than tens of meters in diameter can survive entry into the Earth's atmosphere and cause extensive regional damage (Popova et al. 2013; Mathias et al. 2017). With the aid of large-scale sky surveys such as the Asteroid Terrestrial-impact Last Alert System (ATLAS; Tonry et al. 2018), the Near-Earth Object Wide-field Infrared Survey Explorer (NEOWISE; Mainzer et al. 2011), the Panoramic Survey Telescope and Rapid Response System (Pan-STARRS; Vereš et al. 2015), and the upcoming Vera C. Rubin Observatory, the hunt for potentially hazardous asteroids (PHAs) will continue to increase the fraction of known near-Earth objects (Jones et al. 2018).

The spotlight then switches to what can be done when a PHA is discovered to be on a collision course with the Earth. Ahrens & Harris (1992) proposed an idea for a kinetic impactor spacecraft for deflecting 100 m-sized asteroids, given sufficient notice. This deflection method involves a hypervelocity collision of a spacecraft with the target asteroid. The resulting momentum transfer changes the orbit of an Earth-bound asteroid and prevents an impact. The Asteroid Impact and Deflection Assessment (AIDA) collaboration was created as a joint international effort to demonstrate the viability of this kinetic impactor concept (e.g., Cheng et al. 2016; Michel et al. 2018). AIDA consists of NASA's Double Asteroid Redirection Test (DART) and the Hera spacecraft built by the European Space Agency. The impact of the DART spacecraft on Dimorphos, the smaller component of the (65803) Didymos binary asteroid system, will change its mutual orbital period (Cheng et al. 2020). These changes will be monitored and assessed through remote observation campaigns from the Earth and other space assets. The Hera spacecraft will then be sent to study the consequent changes in the Didymos system about four years after the DART impact (Michel et al. 2022).

The DART spacecraft launched on 2021 November 23 and is set to impact Dimorphos on 2022 September 26. The resulting change in the orbital period of Dimorphos around Didymos will be used to inform future asteroid deflection missions. In addition to the impulse delivered by the spacecraft, the ejecta particles created during the DART impact are expected to contribute toward the overall momentum transfer. This additional momentum imparted by the ejected particles can be quantified in terms of a momentum enhancement parameter (β) and is of particular importance to the DART mission, since it is one of the largest sources of uncertainty in the outcome of kinetic impactor–based deflection missions (Cheng et al. 2020). This β parameter has been shown to be

very sensitive to impact conditions and target properties (e.g., Holsapple & Housen 2012; Bruck Syal et al. 2016; Raducan et al. 2019; Stickle et al. 2022, this focus issue), which are not known prior to the impact in the case of Dimorphos.

The generation of ejecta during a hypervelocity impact has been studied both experimentally and in numerical simulations for various material properties (e.g., Raducan et al. 2019; Luther et al. 2022, this focus issue; Stickle et al. 2022, this focus issue, and references therein). Holsapple & Housen (2012) derived a number of scaling relationships based on laboratory experiments that can be applied to asteroid impacts. However, none of the Earth-based targets act as appropriate analogs of asteroid material, and actual measurements of β in realistic settings are needed to validate numerical models. This is precisely what the community expects from AIDA.

The primary consequence of the DART mission from a planetary defense perspective is the change to the 11.92 hr orbital period of Dimorphos around Didymos (Rivkin et al. 2021). As a result of this, there is also a change in the heliocentric motion of the Didymos system barycenter, which occurs on a longer timescale than the change in the mutual orbit period. Since this mission is a planetary defense technology demonstration, it is useful to understand these heliocentric changes and their effect on future Didymos–Earth close approaches. This can be achieved by projecting the Didymos system's relative state with respect to Earth onto the "B-plane" (e.g., Farnocchia et al. 2019).

Studying encounters between asteroids and terrestrial planets on the B-plane can facilitate close approach analysis, including whether the asteroid will impact the central body (Farnocchia et al. 2019), as well as the location of any resonant returns of the asteroid at a future date (Valsecchi et al. 2003). The B-plane is also a natural frame for studying "keyholes," regions on the B-plane that guarantee a collision at a future close approach (Chodas 1999).

In this work, we aim to understand the changes to future Didymos–Earth close approaches by creating updated B-plane maps of the system barycenter after the DART impact. This approach allows us to determine whether the DART impact could send the Didymos system on a collision course with the Earth. To provide as accurate an assessment as possible given the limited knowledge of the outcome of the DART impact at this stage, we will connect the momentum enhancement parameter to the likely physical properties of Dimorphos and model the ejecta-enhanced momentum exchange between the DART spacecraft and the Didymos system barycenter over a broad range of initial conditions. This information is then used to obtain an accurate image of the Didymos system's location at future close approaches with Earth.

This paper contains a discussion of the momentum enhancement parameter for kinetic impact–based asteroid deflection and presents specific expressions for the DART impact in Section 2. Section 3 then analyzes the physical parameters, such as surface strength and porosity, that influence the momentum enhancement. This is followed by a description of the dynamical simulations used to model the impact on Dimorphos and the consequent path of ejecta leaving the system in Section 4. In Section 5, we describe how the ejecta simulation results are factored in to calculate the Didymos–Earth close approach parameters over the next 100 yr. We analyze how these future close approaches are altered for a variety of DART impact scenarios and discuss their dependence on the momentum enhancement. Finally, Section 6 summarizes these results.

2. The Momentum Enhancement Parameter

A simple model for the change in velocity of the target asteroid in a kinetic impact–based asteroid deflection mission was presented in Feldhacker et al. (2017),

$$\Delta \boldsymbol{V} = \frac{m}{M}[\boldsymbol{V}_\infty + (\beta - 1)(\boldsymbol{V}_\infty \cdot \hat{\boldsymbol{n}})\hat{\boldsymbol{n}}], \tag{1}$$

where m is the mass of the impactor, M is the mass of the target asteroid, $\boldsymbol{V}_\infty$ is the relative velocity of the impactor, β is the momentum enhancement factor, and $\hat{\boldsymbol{n}}$ is the surface normal direction at the site of impact. The first term on the right-hand side of this equation is the contribution of the momentum delivered by the spacecraft on impact, and the second term is the contribution of the escaping ejecta momentum. When this escaping ejecta momentum is assumed to be along the surface normal, β can be written as (Cheng et al. 2020)

$$\beta = \frac{M(\Delta \boldsymbol{V} \cdot \hat{\boldsymbol{n}})}{m(\boldsymbol{V}_\infty \cdot \hat{\boldsymbol{n}})}. \tag{2}$$

For the DART impact, the momentum enhancement experienced by the target Dimorphos in its orbit around the asteroid Didymos is nominally expected to fall within the range $1 \leqslant \beta \leqslant 5$ (Stickle et al. 2022, this focus issue). The primary measurement that will be used to determine the value of β is the period change of Dimorphos around Didymos, ΔP. Rivkin et al. (2021) presented a slightly modified version of the β equation based on the along-track change in Dimorphos's orbital velocity ΔV_T,

$$\beta = \frac{(m_{\rm dim}/m_{\rm DART})\Delta V_T - \boldsymbol{V}_{\infty_{\perp n}} \cdot \hat{\boldsymbol{e}}_T + V_{\infty_n}\boldsymbol{\epsilon} \cdot \hat{\boldsymbol{e}}_T}{V_{\infty_n}(\hat{\boldsymbol{n}} + \boldsymbol{\epsilon}) \cdot \hat{\boldsymbol{e}}_T}, \tag{3}$$

where $m_{\rm dim}$ is the mass of Dimorphos, $m_{\rm DART}$ is the mass of the DART spacecraft at impact, and V_{∞_n} is the impact velocity component in the normal direction ($\boldsymbol{V}_\infty \cdot \hat{\boldsymbol{n}}$). Here, $\boldsymbol{V}_{\infty_{\perp n}}$ is the velocity component orthogonal to the normal direction ($\boldsymbol{V}_\infty - V_{\infty_n}\hat{\boldsymbol{n}}$), $\hat{\boldsymbol{e}}_T$ is the unit vector of Dimorphos's orbital velocity at impact, and $\boldsymbol{\epsilon}$ is the the offset vector between the surface normal direction and the ejecta velocity vector. Equation (3) provides a convenient framework for estimating the β factor in the Didymos–Dimorphos system given the data expected from the DART mission. For a head-on collision, Equation (3) simplifies to

$$\beta = 1 + \frac{p_{\rm ejecta}}{p_{\rm DART}}, \tag{4}$$

where $p_{\rm ejecta}$ is the momentum of the ejecta in the vertical direction, and $p_{\rm DART}$ is the vertical component of the momentum of the DART spacecraft at impact.

In contrast, this work focuses on the heliocentric changes to the entire Didymos system as a result of the DART impact, with particular emphasis on the contribution of possible ejecta leaving the system. Therefore, we model the momentum transfer onto the entire Didymos system as

$$\Delta \boldsymbol{p}_{\rm sys}(t) = \boldsymbol{p}_{\rm DART}(t_0) + \int_{t_0}^{t} \boldsymbol{p}_{\rm ejecta}(\tau) d\tau, \tag{5}$$

where $\Delta \boldsymbol{p}_{\rm sys}(t)$ is the change in momentum of the Didymos system at time t past impact (t_0), and $\boldsymbol{p}_{\rm DART}(t_0)$ is the momentum imparted by the DART spacecraft at impact. Furthermore, $\boldsymbol{p}_{\rm ejecta}(t)$ is the momentum carried by ejecta that is leaving the Didymos system at any given moment. The resulting change in the heliocentric orbit can be characterized by the heliocentric beta parameter, $\beta_{\odot}$, which we define as

$$\Delta \boldsymbol{V} = \beta_{\odot} \frac{\boldsymbol{p}_{\rm DART}}{M_{\rm sys}}. \tag{6}$$

Here, $\Delta \boldsymbol{V}$ represents the integrated change in the velocity of the Didymos system barycenter and $M_{\rm sys}$ denotes the mass of the entire Didymos system.

3. Dependence on Physical Parameters

The mechanical properties of the target asteroid play a crucial role in impact cratering processes and are the main contributors to the magnitude of the local momentum transfer efficiency factor, β. Past impact experiments have shown that the mass–velocity distribution of ejecta is sensitive to target properties and the density and speed of the impactor. These studies include the Gault et al. (1963) experiments, which recorded the mass–velocity distribution of the ejecta from impacts on strong basalt (≈30 MPa); the Housen (1992) experiments, which recorded the ejected mass as a function of the velocity of the ejecta from impacts on weaker material mixtures (<1 MPa); the Housen & Holsapple (2003) experiments that studied impacts on highly porous mixtures of sand and fly ash; and the Cintala et al. (1999) and Anderson et al. (2003) experiments that studied the velocities and angles of ejection from impacts on sand targets.

Using these experiments, point-source approximations, and dimensional analysis, Housen et al. (1983) developed a number of power-law scaling relations that describe the variation in the mass–velocity distribution of the ejecta using initial impact conditions and target properties. To a first-order approximation, these are power-law expressions that deviate at the impact site and the crater rim. For an impactor of radius a, mass m, velocity U, and density δ, the velocity of the ejecta launched at a distance x from the impact site, $v(x)$, is expressed as a power-law equation of the normalized launch position, x/a (Housen & Holsapple 2011):

$$\frac{v(x)}{U} = C_1 \left[\frac{x}{a} \left(\frac{\rho}{\delta} \right)^{\nu} \right]^{(-1/\mu)} \left[1 - \frac{x}{n_2 R} \right]^{p}. \tag{7}$$

The mass of the ejecta ($\mathcal{M}$) launched within a distance x from the impact site is expressed as

$$\frac{\mathcal{M}(<x)}{m} = \frac{3k}{4\pi} \frac{\rho}{\delta} \left[\left(\frac{x}{a} \right)^3 - n_1^3 \right]. \tag{8}$$

Here, C_1, k, n_1, n_2, μ, and ν are target material dependent constants, R is the radius of the impact crater, and ρ is the bulk density of the target at the impact site.

Though each suite of experiments had different impact conditions or target properties, they concluded that the ejecta mass–velocity distribution is most sensitive to target properties such as strength and porosity. However, it is difficult to quantify the influence of these properties independently using laboratory data alone. To improve our understanding of the sensitivity of ejecta mass–velocity distributions to material strength and porosity, several systematic numerical studies have investigated this problem. Such numerical simulations allow for studying a larger range of events that are relevant to planetary science problems compared to laboratory experiments. In the following subsections, we include a brief description of several systematic studies undertaken in the context of the DART impact on Dimorphos.

3.1. Systematic Numerical Studies on the Influence of Physical Parameters on β

One of the most important target properties that influences the evolution of the crater and the production of ejecta is the target yield strength at zero pressure (i.e., cohesion). The influence of the effects of target cohesion on cratering has been studied in several numerical studies (e.g., Bruck Syal et al. 2016; Raducan et al. 2019).

Raducan et al. (2019) used the iSALE-2D shock physics code (Wünnemann et al. 2006; Collins et al. 2011) to numerically simulate impacts on low-gravity, strength-dominated asteroid surfaces with varying target cohesion, coefficient of internal friction, and porosity. Using this, they proposed a revision to the Housen & Holsapple (2011) ejecta scaling relations to better approximate the non-power-law behavior of the high-speed ejecta close to the impact site. They also found that the cohesion and internal friction coefficient of the target asteroid's surface after passage of the shock wave have the greatest influence on the momentum transfer. An increase in target cohesion limits the amount of total ejecta and slows down the last ejecta particles that leave the crater. An increase in internal friction leads to lower ejection velocities. Therefore, as the cohesion or coefficient of internal friction is decreased, the momentum transfer efficiency, β, increases.

While the porosity of Didymos is estimated to be about 20% (Naidu et al. 2020), the porosity of Dimorphos is still uncertain. Systematic studies by Raducan et al. (2019) showed that an increase in the initial porosity of the target leads to lower ejection velocities, which in turn leads to lower β values. For fixed cohesion and coefficient of internal friction, a decrease in target porosity from 50% to 10% leads to an increase in β of 1.5.

Raducan et al. (2019) studied impacts on targets with cohesion between 0.1 and 100 kPa. However, due to the new evidence of very weak asteroid surfaces (e.g., Walsh et al. 2019; Arakawa et al. 2020), this study was extended by Raducan & Jutzi (2022) to impacts on targets with cohesion down to 0 Pa. They found that, when impacting a target with fixed, 40% porosity and $f = 0.6$, the β factor increases from ≈3.5 for a 50 Pa target to $\beta \approx 5$ for a cohesionless 0 Pa target. When varying the coefficient of internal friction (for fixed target cohesion and porosity), they found that an increase from $f = 0.4$ to 1.0 leads to a 25% (50 Pa cases) to 33% (0 Pa cases) decrease in β (Figure 1(b)). Their results and the trends observed in the ejecta mass–velocity distribution from DART-like impacts are in good agreement with the numerical results from iSALE-2D (Raducan et al. 2019) and numerical studies of impacts in the gravity regime (e.g., Prieur et al. 2017; Luther et al. 2018).

3.2. Momentum Distribution in Ejecta

The data from the studies described in Section 3.1 were used to quantify the amount of ejected mass and momentum that

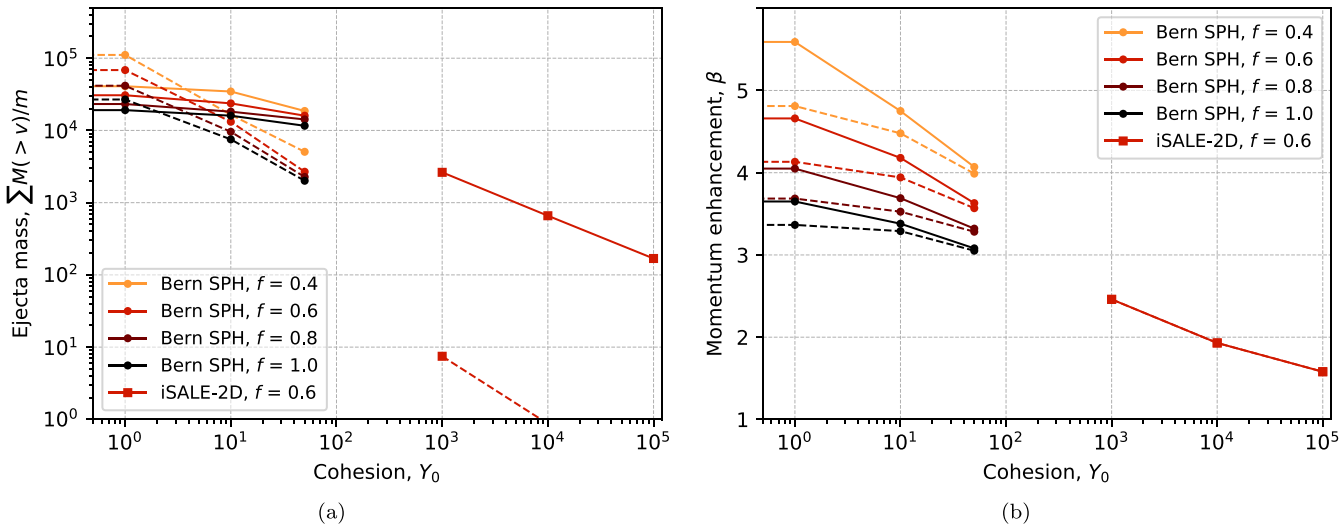

Figure 1. (a) Total ejecta mass from DART-like impacts into asteroid surfaces with varying cohesion, Y_0, and coefficient of internal friction, f, and fixed porosity ($\phi_0 = 40\%$) from Bern SPH (Raducan & Jutzi 2022) and iSALE-2D (Raducan et al. 2019) simulations. The continuous lines show the total amount of ejecta mass that is ejected with velocities higher than the escape velocity of the Didymos system, whereas the dotted lines show the total amount of ejecta mass with velocities lower than the escape velocity of the Didymos system. (b) Momentum enhancement from DART-like impacts into asteroid surfaces with varying cohesion, Y_0, and coefficient of internal friction, f, and fixed porosity ($\phi_0 = 40\%$) from Bern SPH (Raducan & Jutzi 2022) and iSALE-2D (Raducan et al. 2019) simulations. The solid lines show the total momentum enhancement generated by the impact. The dotted lines show the heliocentric momentum enhancement (i.e., the total momentum of the ejecta that leaves the Didymos system).

leaves the Didymos system compared to the amount of mass and momentum that remains within the system, depending on Dimorphos's target properties. The Raducan et al. (2019) study suggested that the influence of the target porosity on impact ejecta production is overcome by the influence of the target strength parameters (i.e., cohesion and coefficient of internal friction). Therefore, in this section, we further focus on data from impacts on targets with fixed porosity and varying cohesion and coefficient of internal friction.

In Figure 1(a), the solid lines show the total mass of ejecta, and in Figure 1(b), the solid lines show the momentum enhancement, β, from impact simulations using the Bern smoothed particle hydrodynamics (SPH) and iSALE-2D codes for targets with constant porosity (40%) and varying cohesion and coefficient of internal friction. For completeness, here we plot the results from both the Bern SPH study (Raducan & Jutzi 2022) and the iSALE-2D study (Raducan et al. 2019). However, there are slight variations in terms of strength and porosity model parameters between the simulations in the two studies, and a direct comparison between the results should be avoided.

We assume that ejected material with velocities lower than 5 cm s^{-1} lands back on Dimorphos and does not contribute to the ejecta mass or momentum enhancement. This escape velocity value was calculated from the currently available estimates for the size and density of Dimorphos from the Design Reference Asteroid v. 3.2 (DART investigation team internal document). Then, we assume that material ejected with speeds lower than the escape velocity of the system, $v_{\rm esc,sys}$, remains trapped within the Didymos system and does not contribute to the heliocentric momentum enhancement. To determine the escape velocity of the system, we use the following approximation:

$$v_{\rm esc,sys} = \sqrt{2G\left(\frac{m_{\rm didy}}{r_{\rm orbit}} + \frac{m_{\rm dim}}{r_{\rm dim}}\right)} \approx \sqrt{2G\frac{m_{\rm didy}}{r_{\rm orbit}}}, \qquad (9)$$

where G is the universal gravitational constant, $m_{\rm didy}$ is the mass of Didymos, $r_{\rm orbit}$ is the average separation between Didymos and Dimorphos, and $m_{\rm dim}$ and $r_{\rm dim}$ are the mass and radius of Dimorphos, respectively. Using this approximation, we find $v_{\rm esc,sys} \approx 24.5$ cm s^{-1}.

We use this speed threshold for particles ejected from the Raducan et al. (2019) and Raducan & Jutzi (2022) impact simulations. In Figure 1(a), the dotted lines show the total amount of ejecta mass that does not escape the Didymos system. As discussed in Raducan & Jutzi (2022), for impacts on strong targets ($Y_0 > \approx$50 Pa), most of the mass is ejected at speeds higher than the escape velocity of the Didymos system. The reason for this is that the ejected material must have a maximum speed that exceeds the escape velocity needed to overcome the cohesive strength of the target (Raducan et al. 2019; Raducan & Jutzi 2022). For impacts into targets weaker than $Y_0 < \approx$10 Pa, the total ejecta mass that remains in the system exceeds the total ejecta mass that leaves the system.

In Figure 1(b), the dotted lines show the heliocentric momentum enhancement (i.e., the cumulative momentum of the ejecta that leaves the Didymos system). The figure shows that the difference between the total and heliocentric momentum enhancement increases with decreasing cohesion. Although for targets stronger than 50 Pa, about 98% of the ejecta momentum leaves the Didymos system, this percentage is reduced to 80% for a cohesionless target ($Y_0 = 0$).

4. DART Ejecta Dynamics Simulations

Before ejecta particles can be placed in an N-body environment to understand the Didymos system's long-term dynamical evolution, initial conditions need to be determined for particles coming off the surface of Dimorphos. The scaling relationships from Equations (7) and (8) are then applied from the impact site to the crater rim to yield initial state information for the ejecta particles. The results presented in this paper correspond to the nominal restricted full three-body problem

Table 1
Dimorphos Mechanical Properties Used for Ejecta Simulation

Parameter	Value
DART effective radius, a	0.5 m
DART mass, m	536 kg
DART impact velocity, U	6143.34 m s^{-1}
DART effective density, δ	1023.69 kg m^{-3}
Dimorphos cohesive strength, Y	100 Pa
Dimorphos porosity, ϕ_0	35%
Dimorphos bulk density, ρ	2202.77 kg m^{-3}
Density scaling exponent, ν	0.40
Velocity scaling exponent, μ	0.41
k	0.30
p	0.30
C_1	0.55
n_1	1.20
n_2	1.00

(RF3BP) ejecta simulation run described in Fahnestock et al. (2022, this focus issue) that used the parameters outlined in Table 1.

In order to propagate impact ejecta particles, both gravitational forces and nongravitational effects such as solar radiation pressure (SRP) need to be considered. Additionally, the gravitational forces near Didymos and Dimorphos cannot simply be calculated by approximating them as point masses due to their irregular shapes. To mitigate these challenges, we used an open-source software package called GUBAS[7] that solves the full two-body problem presented by the binary asteroid system (Davis & Scheeres 2020). Both Didymos and Dimorphos are simulated using shape models that are discretized into polyhedra. Computing the mutual gravitational forces on these polyhedra allows for a high-fidelity dynamical model of the binary asteroid system.

The ejecta particles are then initialized in this environment and propagated without any interparticle interaction. Thus, each particle forms the third body in the RF3BP. The SRP model used in this scenario is a simple cannonball approximation with shadowing. The particle–asteroid gravity, point-mass solar gravity, and SRP accelerations are integrated using a variable-step Runge–Kutta–Fehlberg 7(8) integrator (Fehlberg 1968). The states of those ejecta that escape (per definitions below) Dimorphos and the Didymos system are used to determine β and $\beta_\odot$, respectively. A simulation duration of 20 days was chosen because nearly all of the escaping ejecta have left the system before the 10 day point, and $\beta_\odot - 1$ levels off before this time, as shown in Figure 2(b). The work done in Fahnestock et al. (2022, this focus issue) presents a more detailed description of the efforts to study the ejecta generated by the DART impact.

An analytical expression to approximate β is given by Cheng et al. (2016) by accumulating the ejecta momentum from the impact site to the crater rim. The resulting integral approximation for the momentum enhancement parameter can be written as

$$\beta \approx 1 + \frac{9kC_1}{4\sqrt{2}\pi a}\left(\frac{\rho}{\delta}\right)^{\frac{\mu-\nu}{\mu}} \int_{n_1 a}^{n_2 R} \left(\frac{x}{a}\right)^{\frac{2\mu-1}{\mu}} dx = 1.877. \quad (10)$$

A more convenient approach to determining β that makes the most use of the available information is to directly use the results of the RF3BP simulations and Equation (4) in the form

$$\beta = 1 + \frac{p_{\mathrm{ej,dim}}}{p_{\mathrm{DART}}} = 1.894, \quad (11)$$

where $p_{\mathrm{ej,dim}}$ is the cumulative momentum magnitude of the ejecta particles escaping Dimorphos at the end of crater formation, and p_{DART} is the magnitude of the DART spacecraft's relative momentum at impact. This value shows excellent agreement with the analytical approximation (under 1%), which is consistent with previous studies (Raducan et al. 2019).

The heliocentric $\beta_\odot$ is calculated using the ejecta states at the moment they escape the binary asteroid system. Here "escape" is defined as the moment an ejecta particle crosses the Hill sphere of the asteroid system, the radius of which is calculated as

$$r_{\mathrm{H}} = r_\odot \sqrt[3]{\frac{M_{\mathrm{sys}}}{3M_\odot}} = 70.905 \text{ km}, \quad (12)$$

where $r_\odot$ is the distance from the Sun to the Didymos system barycenter, M_{sys} is the mass of the Didymos system, and $M_\odot$ is the mass of the Sun. Additionally, the cumulative momentum at the exact moment each particle crosses the Hill sphere is needed to compute the heliocentric momentum enhancement. Since the RF3BP integrator gives state information at discrete times, an interpolation scheme is first used to determine the time at which each escaping particle crosses the Hill sphere and then the state of said particles at this time. Using this information, the heliocentric beta parameter can be determined using a slightly modified Equation (4) as

$$\beta_\odot = 1 + \frac{p_{\mathrm{ej,sys}}}{p_{\mathrm{DART}}} = 1.789, \quad (13)$$

where $p_{\mathrm{ej,sys}}$ is the cumulative momentum of the escaping ejecta particles. Figure 2 shows the temporal evolution of the mass and momentum of the escaping particles, as well as the DART-normalized ejecta momentum, i.e., $\beta_\odot - 1$. In the simulation presented in this paper, 88% of the overall ejecta momentum coming off Dimorphos's surface ended up leaving the system, and so did 95% of the mass displaced by the DART spacecraft's impact.

5. Changes to Future Didymos–Earth Close Approaches

To evaluate the changes of the post-DART Didymos orbit, especially during upcoming Earth close approaches, two key pieces of information were extracted from the RF3BP simulation results: (1) the $\beta_\odot$ value from Equation (13) and (2) the time series data of ejecta momentum imparted to the Didymos system's barycenter as presented in Figure 2. These data were used in two different approaches to simulating the DART spacecraft impact; case 1 does this by imparting an instantaneous change in velocity of -1.062×10^{-5} m s^{-1} to the Didymos system barycenter calculated from Equation (6), and case 2 accounts for the ejecta momentum imparted as a function of time past the impact by imparting a change in velocity to the system barycenter when individual ejecta particles escape.

[7] https://github.com/alex-b-davis/gubas

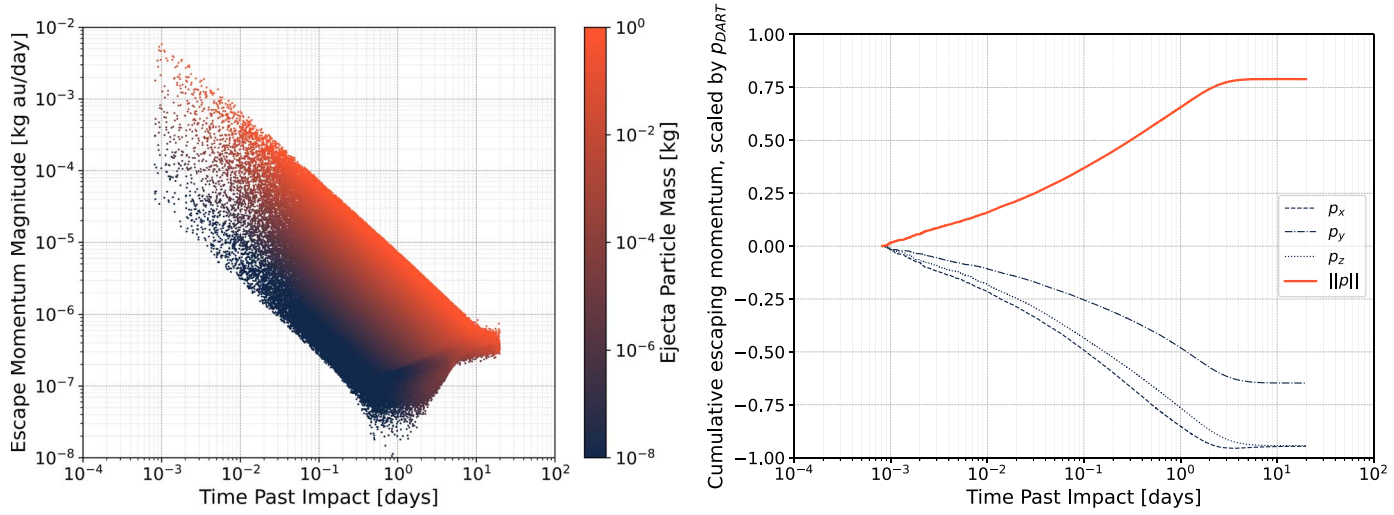

(a) (b)

Figure 2. Summary of ejecta particles that escape the Didymos system. (a) Magnitude of the ejecta particles' momenta at the time of crossing the Hill sphere, colored by the particle mass. (b) Cumulative ejecta contribution to the momentum enhancement parameter ($\beta_\odot - 1$) as a function of time. The components are shown in the International Celestial Reference Frame Earth mean equator frame.

5.1. Didymos Dynamical Model

Table 2 shows the initial conditions and integration parameters used to compute the close approach B-planes of the system after the DART impact for both cases. The initial state and covariance matrix for the Didymos system are taken from the NASA Jet Propulsion Laboratory (JPL) Orbit Solution 181.[8] This information was used to provide the coordinates for a nominal orbit, as well as the associated position uncertainty information on the B-plane using 10^4 Monte Carlo clones generated via a multivariate normal sampling of the covariance matrix from solution 181. Our initial simulations were performed with 10^6 clones. However, we found that the relatively small deflection DART imparts on the Didymos–Earth close encounters leads to a near-linear response in the system. Consequently, using 10^4 clones retained sufficient accuracy while greatly improving computational efficiency in our orbit uncertainty propagation simulations.

The dynamical model used here includes parameterized post-Newtonian formulations of general relativity for the Sun, Earth, and Jupiter, as well as J_2 zonal harmonic contributions from the Sun and Earth. In addition to the Sun and the solar system planets, point-mass gravitational accelerations from the Moon, Pluto, and the 16 most massive main belt asteroid perturbers are also included, as provided by the JPL DE441 and DE441-N16 ephemerides. Solution 181 also contains an estimate for the nongravitational transverse acceleration parameter, A_2. Marsden et al. (1973) and Farnocchia et al. (2013b) used this parameter to approximate the acceleration due to the Yarkovsky effect as

$$\ddot{\boldsymbol{r}}_t = A_2 \left(\frac{1}{r_\odot}\right)^2 \hat{\boldsymbol{t}}, \tag{14}$$

where $\ddot{\boldsymbol{r}}_t$ is the transverse nongravitational acceleration, $r_\odot$ is the distance from the Sun to the Didymos system barycenter, and $\hat{\boldsymbol{t}} = \hat{\boldsymbol{h}} \times \hat{\boldsymbol{r}}$ is the unit vector in the transverse direction, i.e., the cross product between the unit radial ($\boldsymbol{r}$) and orbital angular momentum ($\boldsymbol{h}$) vectors. The influence of the Yarkovsky effect on our investigation, and the consequences thereof, are discussed in Section 5.3.

Table 2
Initial Conditions and Parameters Used for Didymos–Earth Close Approach Calculations

Parameter	Value
Integration start epoch	JD 2 457 380.0
Perihelion distance, q	1.013062336 au
Eccentricity, e	0.383882802
Inclination, i	3.°407768167
Argument of perihelion, ω	319.°233323014
Longitude of the ascending node, Ω	73.°227914765
Time of perihelion passage, T_p	JD 2 457 563.408
Nongravitational transverse acceleration parameter, A_2	$-1.885839515 \times 10^{-14}$ au day^{-2}
Integration span	120 yr
DART impact epoch	JD 2 459 849.469

A new, modified version of the adaptive 15th-order RADAU integrator (Everhart 1985) and the IAS15 integrator (Rein & Spiegel 2014) was developed for the purpose of simulating asteroid impacts for this work. This allows us to account for the momentum imparted by the escaping ejecta particles with high fidelity. This new integrator was used to model the DART impact while propagating the state of the Didymos system barycenter through the integration span specified in Table 2 and calculating any close approaches with the Earth.

To ensure the accuracy of the close approach parameters calculated with this new integrator, the next two Earth close approaches within 0.1 au for the Didymos system were compared to B-plane uncertainty ellipses previously computed at JPL (Chesley & Eggl 2018). Note that these ellipses were generated using JPL solution 134 for validation purposes only. As mentioned previously, solution 181 contains the latest orbit for the Didymos system barycenter and was therefore used to produce the results presented in this work. A comparison between the JPL results and the ones generated using the

[8] JPL Small Body Database Browser (SBDB), https://ssd.jpl.nasa.gov/sbdb.cgi?sstr=didymos. Solution 181 retrieved 2022 March.

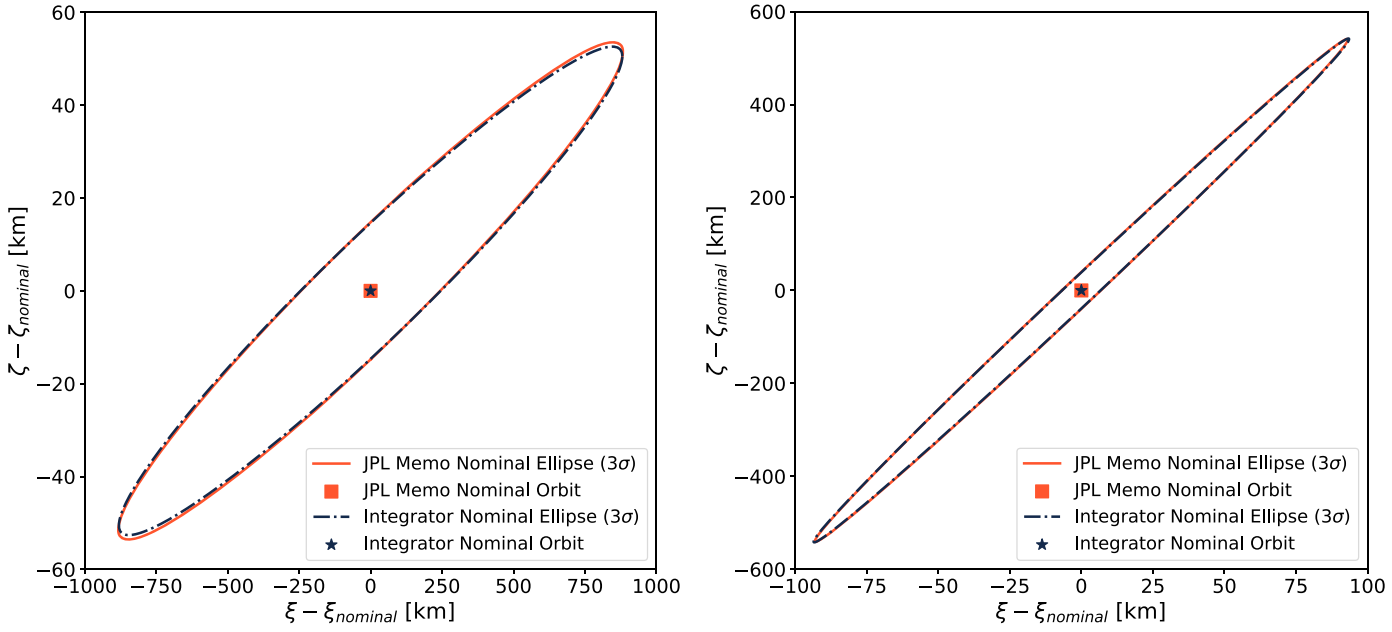

Figure 3. Didymos–Earth close approach uncertainty ellipses for validating the new Gauss–Radau integrator accuracy against results from Chesley & Eggl (2018) during the (a) 2062 October 20 close approach and (b) 2123 November 4 close approach.

aforementioned integrator is shown in Figure 3. The two sets of uncertainty ellipses show excellent agreement with each other in their principal axes and orientation with respect to the B-plane horizontal ($\zeta = 0$), validating the integrator and the dynamical model used in this work.

In both cases of the DART impact simulation, the integrator time step is forced to the DART impact epoch. For case 1, the linear momentum exchange that occurs at the time of DART impact is simply scaled by $\beta_\odot$ to account for the escaping ejecta momentum's contribution to the heliocentric orbit change. For case 2, the change in velocity imparted by the DART spacecraft alone is imparted at the time of impact. A fixed time step of 0.01 days is then used for the first 10 days after impact, and the cumulative escaping ejecta momentum in that 0.01 day period is imparted to the Didymos system barycenter at the end of each step. After these 10 days, the ejecta momentum is cumulatively applied at the end of the adaptive time step chosen by the integrator.

Once the Didymos barycenter has been propagated through the integration period, the system's state with respect to the Earth is computed at every integration step to compute the relative distance and radial velocity with respect to the Earth. A potential close approach window is characterized by the beginning and end of an interval where the radial velocity crosses zero and the relative distance is less than 0.1 au. The bounds of this window and a root-finding algorithm that uses Brent's method are then used to compute the exact time when the close approach occurs, i.e., when the relative radial velocity is zero. The Didymos barycenter state at close approach is then calculated by interpolating the states output by the solar system propagator to the time of close approach. The Öpik frame close approach parameters are then calculated using this relative state information for each Didymos–Earth close approach as described in Farnocchia et al. (2019).

5.2. Didymos–Earth B-plane Changes

The first two close approaches within 0.1 au for the Didymos system after the DART impact occur on 2062 October 20 and 2123 November 4 and are summarized on the B-plane maps shown in Figures 4 and 5, respectively. For the first close approach in 2062, the DART spacecraft alone ($\beta_\odot = 1$) deflects the system by about 56 km. The ejecta contribution takes this value to about 101 km when simulated as a single instantaneous momentum change using $\beta_\odot$ (case 1). However, if the ejecta are not assumed to leave the system instantaneously and instead are modeled to escape at each individual particle's escape time, the deflection is about 97 km (case 2).

A similar trend is observed for the second close approach after the DART impact in 2123. The DART spacecraft alone ($\beta_\odot = 1$) deflects the system on the B-plane by about 35 km in this case. For the instantaneous ejecta momentum exchange in case 1, the deflection is about 63 km. If the ejecta particles are modeled to escape when they cross the Hill sphere, the deflection is about 61 km. For both close approaches, the ratio of deflection between the instantaneous ejecta contribution (case 1) to the DART spacecraft-only deflection is 1.79, which is consistent with the $\beta_\odot = 1.789$ value from Equation (13). However, the corresponding ratio of deflection between the individual ejecta particle impulses (case 2) and the deflection of only the DART spacecraft is $\beta^*_\odot = 1.729$, which gives us the effective heliocentric momentum enhancement experienced by the Didymos system barycenter.

In both cases, imparting the ejecta escape momentum when the particles leave the system (case 2) instead of when the spacecraft impacts (case 1) leads to a 3.3% smaller deflection on the B-plane. This is due to the fact that the cratering event on Dimorphos due to the DART spacecraft can last up to hours, which leads to ejecta escape times ranging from microseconds to weeks, depending on the ejection velocity and particle size. Therefore, when available, it is essential to model kinetic

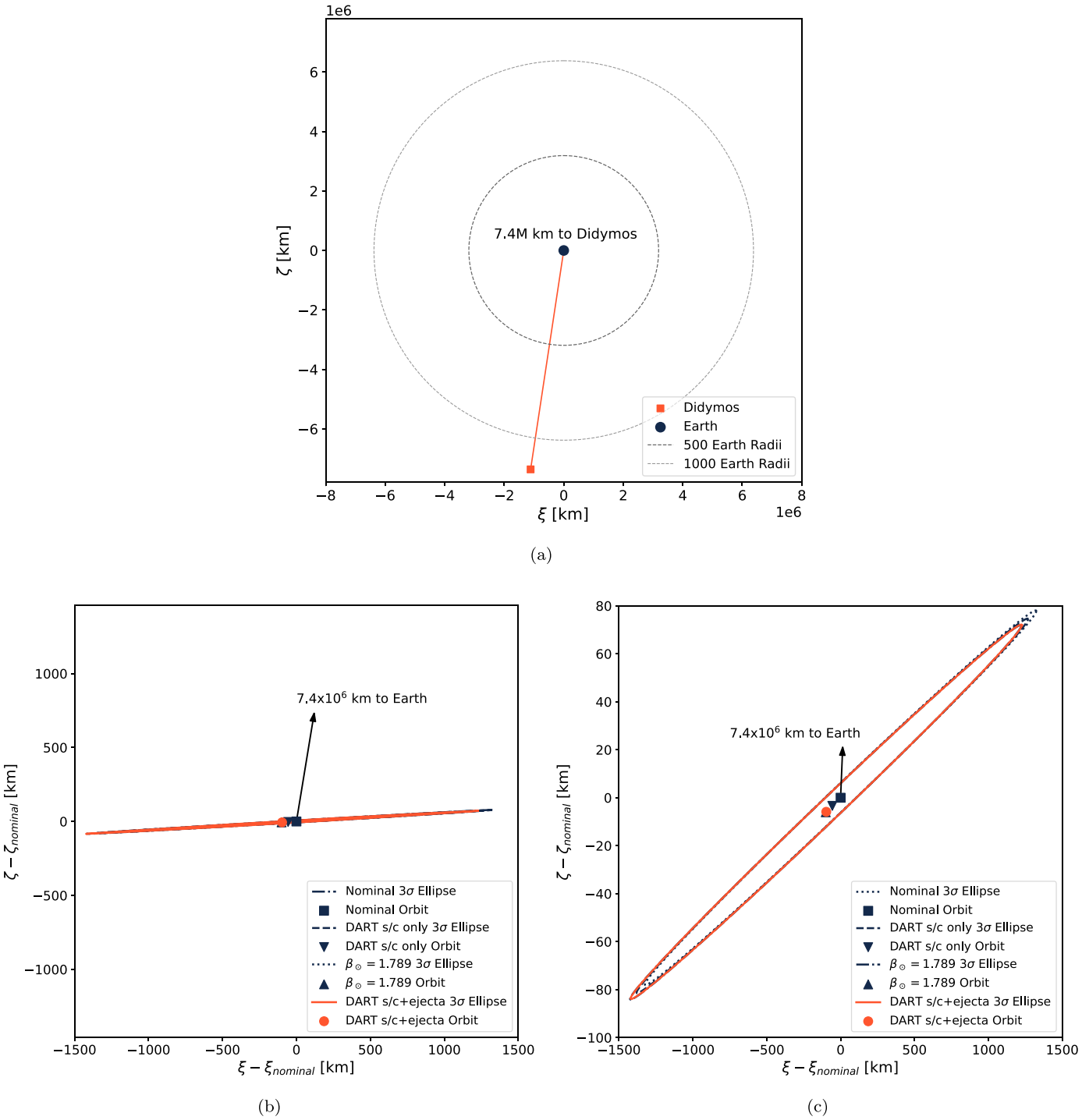

Figure 4. Updated B-plane map for the 2062 October 20 Didymos–Earth close approach. (a) Didymos coordinates on the close approach B-plane shown to scale. (b) Didymos position uncertainty shown to scale on the B-plane for the nominal (no deflection) case, the DART spacecraft contribution only ($\beta_\odot = 1$) case, a single impulse at the time of impact in case 1, and multiple impulses for each escaping ejecta particle in case 2. (c) Didymos position uncertainty zoomed in to show details on the B-plane for the nominal (no deflection) case, DART spacecraft contribution only ($\beta_\odot = 1$) case, single impulse at the time of impact in case 1 ($\beta_\odot = 1.789$), and multiple impulses for each escaping ejecta particle in case 2.

impactor–based deflection campaigns using data for individual escaping ejecta particles for the most accurate predictions about changes to the asteroid's heliocentric orbit.

5.3. Influence of the Yarkovsky Effect

As mentioned in Section 5.1, the A_2 nongravitational transverse acceleration parameter was used in this work to model the acceleration due to the Yarkovsky effect. Here we discuss the influence of modeling the Yarkovsky effect on the position of the Didymos system barycenter during future Earth close approaches. Figure 6 shows the differences in this position for two dynamical models: one that includes the Yarkovsky acceleration (colored ellipses; identical to Figures 4(c) and 5(c)) and another that does not (gray-scale ellipses).

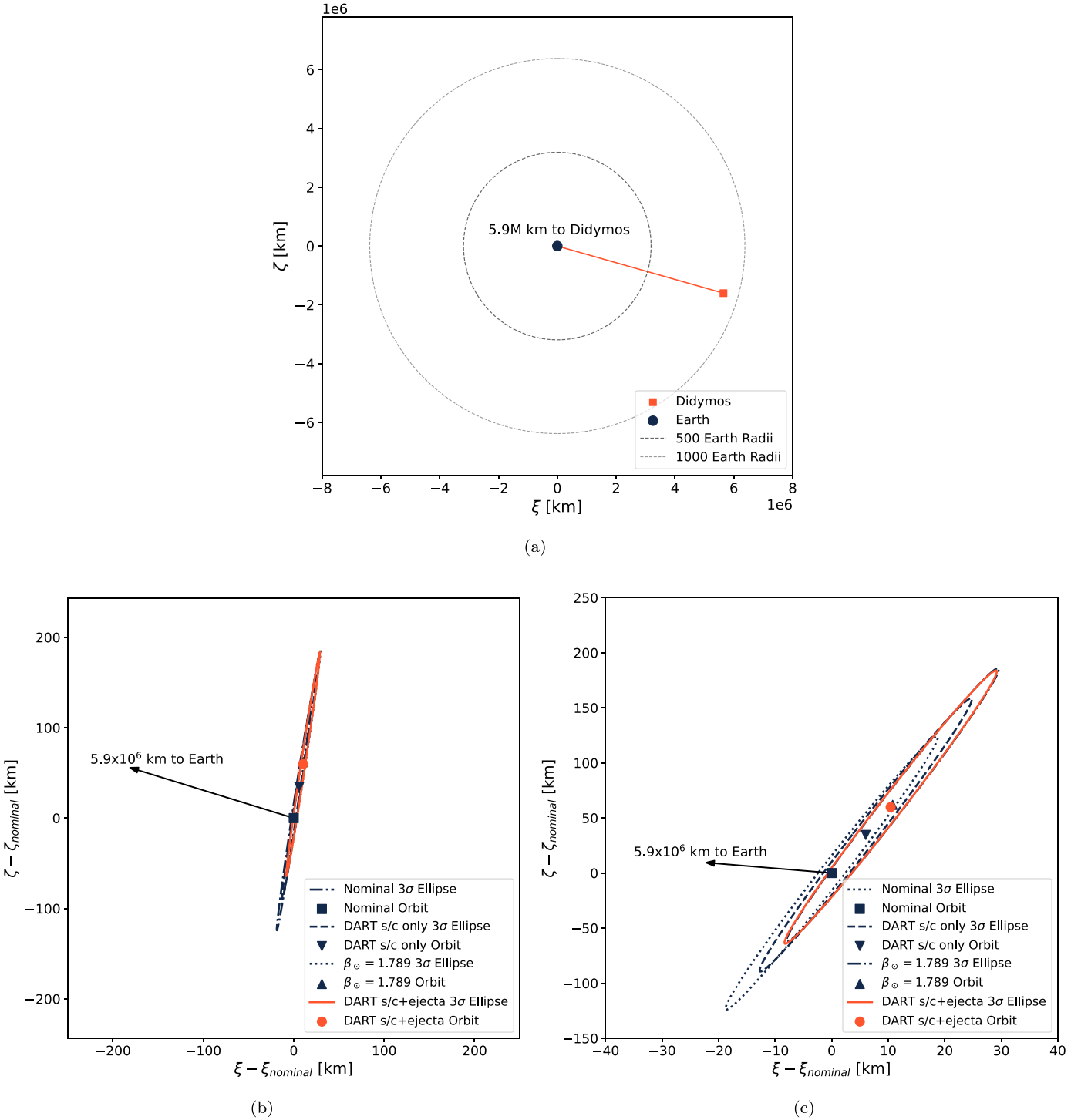

Figure 5. Updated B-plane map for the 2123 November 4 Didymos–Earth close approach. (a) Didymos coordinates on the close approach B-plane shown to scale. (b) Didymos position uncertainty shown to scale on the B-plane for the nominal (no deflection) case, the DART spacecraft contribution only ($\beta_\odot = 1$) case, a single impulse at the time of impact in case 1, and multiple impulses for each escaping ejecta particle in case 2. (c) Didymos position uncertainty zoomed in to show details on the B-plane for the nominal (no deflection) case, DART spacecraft contribution only ($\beta_\odot = 1$) case, single impulse at the time of impact in case 1 ($\beta_\odot = 1.789$), and multiple impulses for each escaping ejecta particle in case 2.

For the 2123 close approach, the difference in including the A_2 parameter could be smaller than the deflection caused by DART, since the two sets of uncertainty ellipses (colored and gray scale) have significant overlap. However, for the 2062 close approach, the difference in B-plane position caused by the inclusion of the Yarkovsky effect significantly dominates the deflection caused by DART. In fact, the gray scale uncertainty ellipses are essentially contained within the colored ellipses that account for the uncertainty in the Yarkovsky effect. This is because the uncertainty in the A_2 parameter (currently 7.227×10^{-15} au day^{-2}) is high enough that adding the 3σ value to the nominal A_2 from Table 2 changes its sign and, consequently, the direction of the acceleration. These plots show the necessity of gathering the additional information

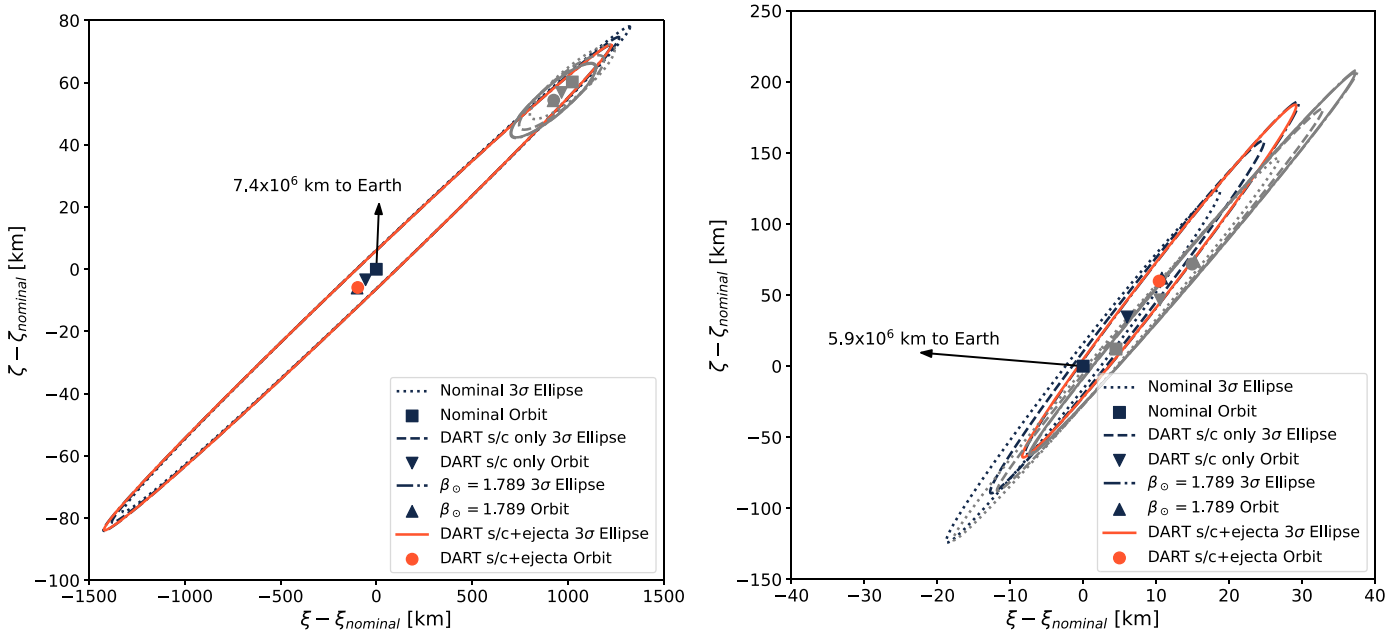

(a) (b)

Figure 6. The B-plane deflections and associated uncertainty ellipses for a dynamical model that includes the Yarkovsky effect (colored) and one that does not (gray scale) for the (a) 2062 October 20 and (b) 2123 November 4 close approaches.

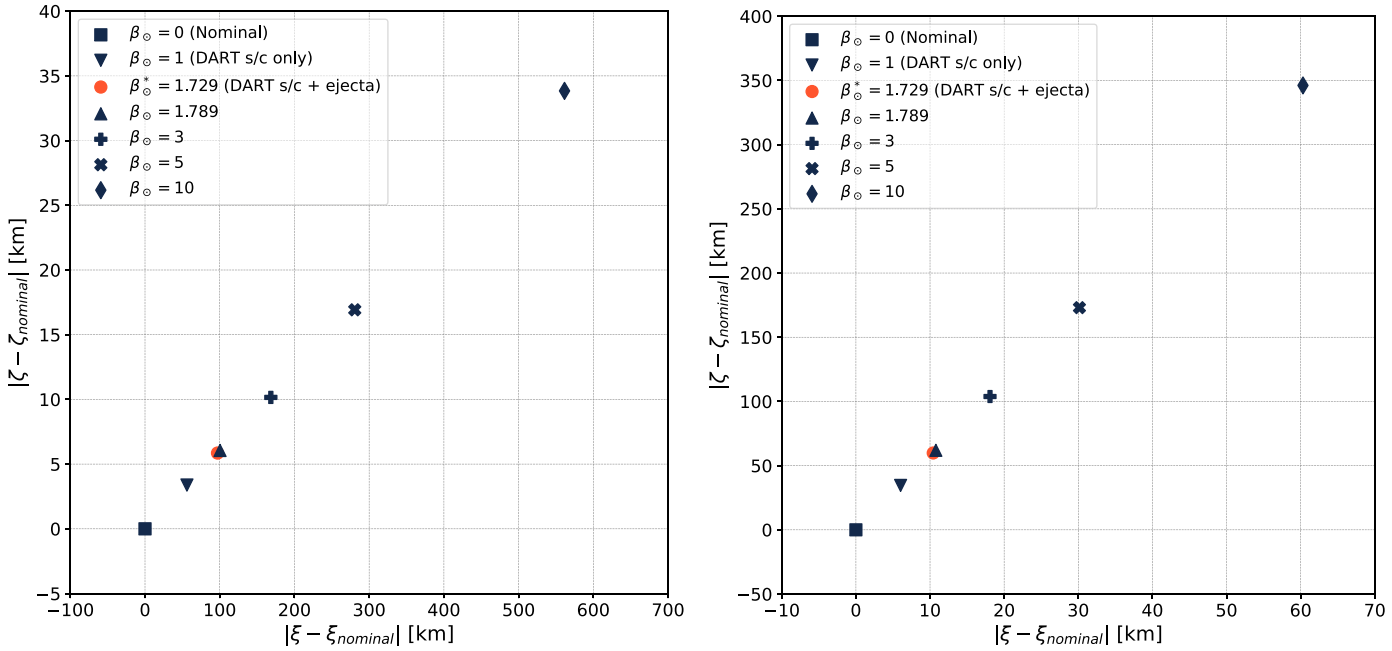

(a) (b)

Figure 7. The B-plane deflections for varying values of $\beta_\odot$ showing a linear increase in deflection magnitude with increasing heliocentric momentum enhancement parameters for the (a) 2062 October 20 and (b) 2123 November 4 close approaches.

needed to reduce the Yarkovsky effect uncertainty for the Didymos system if the changes imparted by the DART impact on the heliocentric orbit of the system are to be constrained from future observations of the heliocentric orbit of the system.

5.4. *Influence of High* $\beta_\odot$ *Values*

To further understand the effects of $\beta_\odot$ on the Didymos system, additional cases similar to case 1 were run, with $\beta_\odot$ values of 3, 5, and 10. This was done to observe the overall trends in B-plane coordinate changes for unexpectedly high heliocentric momentum enhancement parameters. The results in Figure 7 show that the magnitude of the deflection scales linearly with $\beta_\odot$, and that even for an extremely high momentum enhancement provided by the escaping ejecta (nine times the DART spacecraft itself in the $\beta_\odot = 10$ case), the deflection would be on the order of hundreds of kilometers. This is much smaller than the scale of millions of kilometers at

which the close approaches occur. Therefore, the DART impact would not directly send the Didymos system onto a collision course with Earth.

However, another way in which the DART impact could send the Didymos system on a collision course is if a keyhole is triggered on a close approach B-plane. If the asteroid passes through a keyhole at a given close approach, it is guaranteed to impact at a future close approach. Keyholes appear on the B-plane at the intersection of the orbit uncertainty region and a Valsecchi circle (Farnocchia et al. 2013a). Performing this analysis for a nominal Didymos showed that there are no Valsecchi circles near Didymos's B-plane coordinates in 2022 (which is the close approach near which the DART impact occurs). Additionally, performing the same analysis for the post-DART close approaches in 2062 and 2123 calculated using our numerical integrator showed the same results, ruling out the possibility of triggering keyholes due to the DART impact. As an additional layer of safety, a cloud of 10^6 quasi-random, uniformly sampled Monte Carlo clones within a $10^5-\sigma$ bound was propagated through the integration span using the initial covariance information. The results showed that none of these clones got within five lunar distances (more than 300 Earth radii) of the Earth, further indicating that the probability that the Didymos system collides with the Earth is negligible.

6. Summary and Conclusions

In this work, we present a novel methodology to account for momentum transfer of escaping ejecta in kinetic impactor–based asteroid deflection missions. We have applied this methodology to assess the expected change in the heliocentric orbit of the (65803) Didymos binary asteroid system as a consequence of the DART mission.

We found that the nominal orbit of Didymos will likely be shifted on the order of hundreds of kilometers by the DART impact. The precise value of this deflection will be measured once more information about the generated ejecta is available after the impact on 2022 September 26. However, a parametric analysis of the heliocentric momentum enhancement showed that even for an unexpectedly high deflection, Didymos will not be shifted into a collision course with the Earth as a result of the DART impact.

Furthermore, we observed a difference between modeling the ejecta contribution to this deflection campaign as an individual impulse at the time of impact and the more sophisticated approach presented in this work. This difference was found to be ≈3.3% of the overall shift of the Didymos system on the Didymos–Earth B-plane caused by DART. A difference of this magnitude can become significant in the presence of gravitational keyholes.

Therefore, we propose that accurate models of the momentum carried by escaping ejecta over time should be used in the planning of future kinetic impact–based deflection missions.

Moreover, Raducan & Jutzi (2022) showed that there is a correlation between the amount of momentum that is trapped in the system and the impact outcome. They found that in impact scenarios where target deformation occurs, more than ≈7% of the momentum stays in the system. This can lead to an observable difference between β and $\beta_\odot$, depending on the asteroid strength. In the absence of a direct observation of the asteroid cohesion and/or post-impact deformation, an observed significant difference between β and $\beta_\odot$ could imply that Dimorphos is very weak.

Since the acceleration due to the Yarkovsky effect can dominate the B-plane changes caused by DART, we argue the need for a precise determination of the Yarkovsky effect acceleration acting on the Didymos system to allow better constraints on the value of $\beta_\odot$. Work done to explore the observability of $\beta_\odot$ by the authors, in addition to the expected β estimate from the DART Investigation Team, is presented in Richardson et al. (2022). These results show that given the right number of post-DART stellar occultation observations of the Didymos system, an independent estimate for $\beta_\odot$ can be produced. Then, the estimates for both β and $\beta_\odot$ could be used together to reduce the uncertainties about the mechanical properties of Dimorphos. This would be especially helpful for future modeling of the DART impact. It could also aid a future scenario in which additional scouting spacecraft cannot be sent before the impactor spacecraft. In this case, this information would be used to reduce the epistemic uncertainties surrounding a target asteroid's physical properties and allow for accurate predictions of the post-impact heliocentric state of the asteroid.

This work was supported in part by the DART mission, NASA contract No. 80MSFC20D0004 to JHU/APL. S.D.R. acknowledges funding support from the European Union's Horizon 2020 research and innovation program under grant agreement No. 870377 (project NEO-MAPP). E.G.F. acknowledges that some of this research was carried out at the Jet Propulsion Laboratory, California Institute of Technology, under a contract with the National Aeronautics and Space Administration (No. 80NM0018D0004). The authors thank Davide Farnocchia, as well as an anonymous referee, for their insightful suggestions that greatly improved this work.

ORCID iDs

Rahil Makadia https://orcid.org/0000-0001-9265-2230
Sabina D. Raducan https://orcid.org/0000-0002-7478-0148
Siegfried Eggl https://orcid.org/0000-0002-1398-6302

References

Ahrens, T. J., & Harris, A. W. 1992, Natur, 360, 429
Anderson, J. L. B., Schultz, P. H., & Heineck, J. T. 2003, JGRE, 108, 5094
Arakawa, M., Saiki, T., Wada, K., et al. 2020, Sci, 368, 67
Bruck Syal, M., Michael Owen, J., & Miller, P. L. 2016, Icar, 269, 50
Cheng, A., Michel, P., Jutzi, M., et al. 2016, P&SS, 121, 27
Cheng, A. F., Stickle, A. M., Fahnestock, E. G., et al. 2020, Icar, 352, 113989
Chesley, S. R., & Eggl, S. 2018, Post-Deflection Impact Risk Assessment of DART Mission JPL IOM 392-18-003, JPL, Zenodo:10.5281/zenodo.1435957
Chodas, P. W. 1999, BAAS, 31, 1117
Cintala, M. J., Berthoud, L., & Hörz, F. 1999, M&PS, 34, 605
Collins, G. S., Melosh, H. J., & Wünnemann, K. 2011, IJIE, 38, 434
Davis, A. B., & Scheeres, D. J. 2020, Icar, 341, 113439
Everhart, E. 1985, in IAU Coll. 38, Dynamics of Comets: Their Origin and Evolution (Cambridge: Cambridge Univ. Press), 185
Fahnestock, E. G., Cheng, A. F., Ivanovski, S., et al. 2022, PSJ, in press
Farnocchia, D., Chesley, S., Chodas, P., et al. 2013a, Icar, 224, 192
Farnocchia, D., Chesley, S., Vokrouhlický, D., et al. 2013b, Icar, 224, 1
Farnocchia, D., Eggl, S., Chodas, P. W., Giorgini, J. D., & Chesley, S. R. 2019, CeMDA, 131, 36
Fehlberg, E. 1968, Classical Fifth-, Sixth-, Seventh-, and Eighth-Order Runge-Kutta Formulas with Stepsize Control, NASA TR R-287, NASA https://ntrs.nasa.gov/citations/19680027281
Feldhacker, J. D., Syal, M. B., Jones, B. A., et al. 2017, JGCD, 40, 2417

Gault, D., Shoemaker, E., Moore, H., et al. 1963, Spray Ejected from the Lunar Surface by Meteoroid Impact, NASA TN D-1767, NASA https://ntrs.nasa.gov/citations/19630004711
Granvik, M., Morbidelli, A., Jedicke, R., et al. 2018, Icar, 312, 181
Holsapple, K. A., & Housen, K. R. 2012, Icar, 221, 875
Housen, K. R. 1992, LPSC, 23, 555
Housen, K. R., & Holsapple, K. A. 2003, Icar, 163, 102
Housen, K. R., & Holsapple, K. A. 2011, Icar, 211, 856
Housen, K. R., Schmidt, R. M., & Holsapple, K. A. 1983, JGR, 88, 2485
Jones, R. L., Slater, C. T., Moeyens, J., et al. 2018, Icar, 303, 181
Luther, R., Zhu, M.-H., Collins, G., & Wünnemann, K. 2018, M&PS, 53, 1705
Luther, R., Raducan, S. D., Burger, C., et al. 2022, PSJ, submitted
Mainzer, A., Grav, T., Bauer, J., et al. 2011, ApJ, 743, 156
Marsden, B. G., Sekanina, Z., & Yeomans, D. K. 1973, AJ, 78, 211
Mathias, D. L., Wheeler, L. F., & Dotson, J. L. 2017, Icar, 289, 106
Michel, P., Kueppers, M., Sierks, H., et al. 2018, AdSpR, 62, 2261
Michel, P., Küppers, M., Bagatin, A. C., et al. 2022, PSJ, 3, 160
Naidu, S. P., Benner, L. A. M., Brozovic, M., et al. 2020, Icar, 348, 113777
Popova, O. P., Jenniskens, P., Emel'yanenko, V., et al. 2013, Sci, 342, 1069
Prieur, N. C., Rolf, T., Luther, R., et al. 2017, JGRE, 122, 1704
Raducan, S., Davison, T., Luther, R., & Collins, G. 2019, Icar, 329, 282
Raducan, S. D., & Jutzi, M. 2022, PSJ, 3, 128
Rein, H., & Spiegel, D. S. 2014, MNRAS, 446, 1424
Richardson, D. C., Agrusa, H. F., Barbee, B., et al. 2022, PSJ, 3, 157
Rivkin, A. S., Chabot, N. L., Stickle, A. M., et al. 2021, PSJ, 2, 173
Stickle, A. M., Burger, C., Caldwell, W. K., et al. 2022, PSJ, submitted
Tonry, J. L., Denneau, L., Heinze, A. N., et al. 2018, PASP, 130, 064505
Valsecchi, G. B., Milani, A., Gronchi, G. F., & Chesley, S. R. 2003, A&A, 408, 1179
Vereš, P., Jedicke, R., Fitzsimmons, A., et al. 2015, Icar, 261, 34
Walsh, K. J., Jawin, E. R., Ballouz, R.-L., et al. 2019, NatGe, 12, 242
Wünnemann, K., Collins, G. S., & Melosh, H. J. 2006, Icar, 180, 514